TITLE PAGE

TITLE

Mouse navigation strategies for odor source localization

RUNNING TITLE

Odor source localization by mice

AUTHOR NAMES AND AFFILIATIONS

Liu, Annie[1,4*], Papale, Andrew E[1*], Hengenius, James[2*], Patel, Khusbu[3], Ermentrout, Bard[2,4], and Urban Nathaniel N[1,4]

[*] These three authors contributed equally to this manuscript

1. Department of Neurobiology, University of Pittsburgh School of Medicine, Pittsburgh, PA
2. Department of Mathematics, University of Pittsburgh, Pittsburgh, PA
3. University of Pittsburgh, Pittsburgh, PA
4. Center for the Neural Basis of Cognition, Pittsburgh, PA

AUTHOR CONTRIBUTIONS

JH, AL, BE, and NNU designed the behavioral experiments. AEP, JH, BE, and NNU designed the simulations. AL and KP conducted the behavioral experiments. AEP, JH, and AL analyzed the data. AEP and JH wrote the MATLAB code. AEP calculated the statistics. AEP, JH, AL, BE, and NNU wrote the paper.

CORRESPONDING AUTHOR

Andrew E. Papale

papalea@pitt.edu

KEYWORDS

Olfaction, navigation, casting, stereo-olfaction, stereo-sniffing, serial-sniffing

SUMMARY STATEMENT

Use of a naturalistic odor-source localizing task uncovers key strategies underlying successful mouse navigation. Concentration-dependent models successfully recapitulate mouse behavior and reveal important behavioral components.

ABSTRACT

Navigating an odor landscape is a critical behavior for the survival of many species, including mice. One ethologically relevant mouse behavior is locating food using odor concentration gradients. To model this behavior, we use a naturalistic open field odor-based spot-finding task, examining navigation strategies as mice search for and approach an odor source. Mice were trained to navigate to odor sources paired with food reward. We detected behavioral changes consistent with localization of the odor source when mice were ~10cm away from the source. These behaviors included both orientation towards the source and increased exploration time. We found that the amplitude of ‘casting,’ lateral back and forth head movement, increased exponentially with proximity to the source. We then created concentration-dependent models to simulate mouse behavior, which provided evidence for a serial-sniffing strategy (sampling concentration, moving in space, then sampling again) and a stereo-sniffing strategy (inter-nostril comparison of concentration in a single sniff). Together, these results elucidate key components of behavioral strategies for odor-based navigation.

INTRODUCTION

The ability to sense and traverse an odor landscape is critical for the survival of many animal species, facilitating behaviors such as food localization or predator avoidance. Mice, insects, and other animals can navigate odor trails and locate odor sources with high fidelity, a remarkable feat given the complex and variable structure of odor stimuli. Prior studies of olfactory navigation have focused on the mechanisms of navigating through odor plumes in air (Gire et al., 2016; Vickers, 2000) or water (Koehl et al., 1995), or of scent-tracking on the ground, specifically following odor trails (Khan et al., 2012; Means et al., 1992; Porter et al., 2007; Thesen et al., 1993; Wallace et al., 2002). In this study, we examine the odor-driven behaviors involved in the search for a discrete odor object and develop models of olfactory navigation to describe multiple strategies used for effective odor localization.

Broadly, navigation relies on the modification of behavior based on internal motivations and sensory cues. One general strategy preserved across species involves the use of lateral back-and-forth changes in orientation during active odor-sampling (Baker et al., 2018). Moths navigating odor plumes use this strategy to reacquire an odor plume, a behavior termed “zig-zagging” or “casting” depending on the magnitude and angle of displacement (Cardé and Willis, 2008; Kennedy, 1983; Kuenen and Cardé, 1994; Marsh et al., 1978). Flies (Budick and Dickinson, 2006) and cockroaches (Willis et al., 2008) use a similar casting behavior during plume navigation. Similar types of lateral back-and-forth behaviors are observed in animals following discrete odor trails. Rats employ head oscillations that sweep back and forth across a trail as they track it (Khan et al., 2012), a strategy also used by humans (Porter et al., 2007) and ants (Draft et al., 2018; Hangartner, 1969). In this study, we use the term “casting” to describe the head movements observed during mouse odor source localization.

Successful navigation of a complex odor environment likely involves multiple behavioral strategies at different times. Knowledge of the odor environment, characteristics of odor cues, and behavioral decisions required by task decision all influence odor-guided behavior. Animals demonstrate strategy switching between distinct behaviors as a consequence of both changes in odor stimulus and task context (Gire et al., 2016; Pierce-Shimomura et al., 1999; Thesen et al., 1993; Wesson et al., 2008). For example, dogs demonstrate three phases of trail following: an initial search phase (where does the trail start?), a slower direction-finding phase (which direction does the trail go?), and a faster trail-tracking phase (Thesen et al., 1993). Odor source localization, which is an important strategy used by foraging rodents (Gire et al., 2016), may be comparable to the search phase of trail following behavior in dogs. Familiarity with the environment and the presence of visual cues also influences decision-making strategy during odor source localization. After several days of training in the presence of visual landmarks, mice will switch from their initial reliance on sampling of odor cues to identify the source of an odor stimulus to systematic sampling of a small number of known stimulus locations based on some form of memory-based navigation (Gire et al., 2016). This resembles the transition from exploration to exploitation behavior observed during successive search trials across many different types of paradigms (Hills et al., 2015). During this transition, exploratory casting disappears, and mice instead navigate directly to an odor source in straight line trajectories (Bhattacharyya and Bhalla, 2015; Gire et al., 2016). Thus, both behavioral context and stimulus features are important to strategy choice in successful navigation.

It is not yet known if mice use multiple odor-guided strategies for odor source localization when provided with no prior knowledge of source location. Here, we use an open field task to examine the behaviors involved in olfactory search for an odor source. By randomizing odor source location, running trials in the dark, and using a discrete target odorant object, we eliminate visual and auditory cues and prevent mice from switching to methods of systematic search. As we found little evidence for between-trial behavioral differences, it can be inferred that mice are largely using olfactory cues throughout these experiments, allowing us to examine the strategies involved in naturalistic olfactory search. We find that during this task, multiple dimensions of behavior are varied by mice as they approach the odor source. Lastly, we create an agent-based model of olfactory search and use simulations to interrogate the roles of stereo-sniffing, concentration-dependent velocity, and concentration-dependent casting on effective odor localization. Both behavioral and simulation data suggest that multiple behavioral strategies are important for successful odor navigation to an odor source.

MATERIALS AND METHODS

Ethical approval. All experiments were completed in compliance with the guidelines established by the Institutional Animal Care and Use Committee of the University of Pittsburgh.

Animals. Four male and one female adult M72-IRES-ChR2-YFP knock-in mice (*Mus musculus)* (N=5) were used for this study, with training begun after age P47. Average age at training start was P72. All mice were housed singly with behavioral enrichment (running wheel and house) and received unlimited access to water in their home cage.

Behavioral arena. A large, clear behavioral arena was used for data collection, as described in Jones and Urban, 2018 (Jones and Urban, 2018) (Fig. 1A). The arena is a custom built 36” x 45” plexiglass and acrylic surface without walls mounted 4 feet above the floor in an aluminum frame. Rows of infrared light-emitting diodes (LEDs, environmentallights.com) were mounted along each of the four table surface edges. Data were collected using a camera mounted below the table surface (1280x1024 resolution, 50 frames s^{-1}, Flea3, Point Grey Imaging). Trials were run in the dark and electronic LEDs from equipment in the room were blacked out with electrical tape. Remaining light in the behavioral room from computer monitors was red-shifted so as to not be visible to the mice.

Odorized crayon. We created odorized wax crayons similarly to what was described in (Jones and Urban, 2018). Briefly, 4.9 g of a Crayola crayon, 0.1 g of Crayola chalk, and 0.1 g of odorant consisting of one of three different concentrations (0.1%, 1%, and 2% by weight) of methyl salicylate (Sigma-Aldrich) diluted in mineral oil (Fisher Chemical Paraffin Oil, 0121-1) were mixed together, and the mixture was poured into a silicon or rubber crayon mold. After ten minutes, the mixture cooled and hardened into an odorized crayon.

Task: Prior to each trial, the table was wiped clean with 200 proof ethanol using a paper towel. After the table dried, a spot approximately 1.5 cm in diameter was drawn in a pseudorandom location in the central area of the table (Fig. 1B). Based on recent spot placements, the experimenter attempted to place the spot at a different location each subsequent trial. For baited trials, a small piece of chocolate or peanut (~0.1 g) was placed in the middle of the spot, while for unbaited trials, the spot was left empty. With the lights off, a mouse was placed onto the table at a pseudorandom starting location along the right side of the table and allowed to freely explore the arena for approximately 3 minutes. Over the course of 5 months, 133-197 trials were collected per animal, 3-5 trials per day, 3-5 days per week, at a time between 9 am and 2 pm on a normal light-dark cycle. No more than 2 unbaited trials were run on a given day to prevent extinction of behavior.

Food deprivation and task training. To motivate mice to perform the task, they were food deprived to 80-90% of original body weight. Animals received between 1.8-2.2 g of mouse chow per day and were given free access to water. Animals were trained to associate a spot of odor (~1.5 cm diameter) with food reward, either a small sliver of peanut or milk chocolate. Training consisted of two stages: 1) habituation and 2) odor-reward association. During habituation, mice were placed on the table for one 15 minute long trial on two consecutive days and allowed to explore the arena; no food reward was present. During initial food-odor association, plexiglass dividers were used to decrease the arena size (25% of full arena). An odor spot with a food reward was placed on the table. Once animals found the baited spot in the small arena during at least 66% of the day's trials, the arena size was increased to 50% the size of the full arena, followed by an increase to the full 45" x 36" arena once the spot was again found during 66% of the day's baited spot trials. Unbaited spot finding trials were introduced when the animals successfully performed the baited spot task in the full arena. Training ended and data collection began upon successful performance of unbaited

spot trials, which occurred following 6-13 days of training (18-39 trials). All reported data are from the full sized arena, but contain both baited and unbaited trials.

Video Processing. 44 trials were removed from analysis for technical reasons, leaving N=915 trials analyzed. Trials were removed if 1) the video file was corrupted; or, 2) tracking the mouse using Optimouse (see below) was judged by the experimenter to be unsuccessful before data analysis began. This likely occurred due to variation in table illumination on different trials. Of these 915 trials, 54 had odor spot placement within 4 cm of the edge, and were removed from further analysis due to potential obstruction of mouse trajectories near the spots. Finally, 5 trials were removed because the mouse found the spot within 1 s, indicating that it was initially placed on the arena too close to the odor spot (most trials where this occurred the mouse started within 10 cm of the odor spot). This left N=853 trials analyzed here. Raw avi formatted files were processed using the Optimouse open source program (Ben-Shaul, 2017) to extract body position and nose position. The center of mass of the mouse and its nose position were determined post-hoc using Optimouse starting from the time the experimenter's hand was withdrawn from the table. Parameters of 3 or 7 iterations (peels) to remove the mouse's tail and a threshold of 0.5-1 were used with the geodesic distance to compute nose position, with a 'bright mouse' and median background image subtraction. For some trials custom background medians were defined based on frames where the mouse was not in the field of view of the video camera. Extracted position files were then post-processed with in-house software written in Matlab (www.mathworks.com). Position frames were then passed through a 5th order median filter to suppress jitter in the position data. Position data was excluded if 1) Optimouse failed to detect a position, 2) the $\log_{10}$ of mean mouse brightness was less than 0.5 times the mean for that trial, 3) if mean velocity was greater than 100 cm s^{-1}, 4) if the mouse length was greater than 8 cm, 5) if the mouse position 'jumped' by more than 35 pixels (3.13 cm) between consecutive frames, and 6) if the mouse position was 4 cm or closer from the edge of the arena. Note that the edges of the arena were metal fasteners and the mouse was often partially obscured from below when it walked around the edges. Exclusion criteria 6) accounted for the majority (N= 6E6; 84%) of excluded frames, as mice spent a good deal of time at the edges of the arena. Finally, a nearest neighbor filter was used to remove times when the mouse was stationary as the computation orientation of the mouse was unstable. For the majority of analyses, we focused on either the time before a spot was found, or a matched sample of times for unsuccessful trials. A total of 343,177/8E6 position frames (4.26%) were included in the analyses of Figure 3. A total of 1,043,870 frames were used in the analysis of Figure 2C, including frames

where the mouse was paused as determined by the nearest neighbor filter. The distribution of unanalyzed frames was not even across a trial but increased after about 20-30 s when mice began exploring the edges of the arena more frequently.

Data Analysis. A successful spot trial was scored when the mouse's nose came within 1.5 cm of the spot. Varying the capture threshold from 1 cm to 5 cm produced similar results but may have led to increased false positives. A near miss was defined as a trial in which the mouse's nose came within 10 cm of the spot but not within 1.5 cm of the spot. The fractional occupancy was analyzed by defining 50 circular rings around the odor spots at intervals of ~2 cm. The number of samples in each ring was normalized by the total number of samples in the trial to get a measure of the fractional occupancy in each ring for each trial. For trials when the mouse failed to find the odor source, a matched number of samples was taken equal to the number of samples in the last correct trial. As a control, position samples from the correlated random walk (CRW) model were used (see below). To compute the probability of successfully finding an odor source as a function of distance, the occupancy was divided into successful trials (hits) and unsuccessful trials (misses). The fraction of hits was divided by the total number of trials (hits + misses) and averaged across mice. The percentage of time exploring the center of the arena (excluding 4 cm around the edges) was calculated. The fraction of the arena explored was calculated by binning the arena into approximately equal-area parts of (N=9-10,000 partitions). The orientation relative to the odor spot was calculated by computing the arccosine of the dot product between the vectors from body-to-spot and body-to-nose divided by their magnitudes.

Casting behavior was quantified by computing the numerical derivative of the arctangent of the nose velocity in <y> over the nose velocity in <x> divided by the linear velocity of the nose (dPhi/nV). This is a modification of the zIdPhi measurement (Papale et al., 2012). dPhi/nV is equivalent to the signed curvature formula with units of m^{-1} and is therefore an appropriate measure of tortuosity. Derivatives of <x> (x', x'') and <y> (y', y'') were computed using the adaptive windowing Janabi-Sharifi algorithm (Janabi-Sharifi et al., 2011) available online (Manurung, 2016), but modified to handle missing data points (NaNs) and to allow for post-smoothing. Parameters used were a window size of 50 (1 s) and an error term of 0.2, with post smoothing of 0.1 s. The algorithm was extensively tested on variable-frequency sine waves to verify that segments of high curvature were well-separated from segments of high linearity across a wide range of frequencies. Then, for position data from mice, the $\log_{10}$ of the absolute value of dPhi/nV was taken to generate

a roughly normal distribution. An example of the dPhi/nV casting measure (Fig. 1C) for one analyzed behavioral trial shows ‘elbows’ and angled segments with high curvature well-separated from straight segments of high linearity.

An alternate measure of casting used was the deflection distance of the nose relative to the midline. For this measure, the distance from the nose to the midline was determined by calculating a vector for the mouse’s current heading and computing the shortest distance from the detected nose point to that line.

Model Specification. Based on observations of mouse behavior, we developed an agent-based model that navigated a virtual odor environment. This agent made temporally discrete sniff-to-sniff comparisons of odor concentration as it moved through virtual space, altering its heading toward higher concentrations and away from lower concentrations. The agent consisted of a body with coordinates (x, y) and moved through space along a heading θ at a velocity v_c:

$$x_{t+\Delta t} = x_t + v_c\, \Delta t\, cos\, \theta \tag{n1}$$

$$y_{t+\Delta t} = y_t + v_c\, \Delta t\, sin\, \theta \tag{n2}$$

where Δt=0.1 s represents a constant the inter-sniff interval. The agent’s nose was located at a distance ℓ=5 cm from the body at coordinates (x_n, y_n). The nose was further divided into left and right nares, (x_{nL}, y_{nL}) and (x_{nR}, y_{nR}), separated by an inter-nares distance, d_{nares}=1.8 mm. The two nares are separated by an angle γ. The nose was capable of limited movement independent of the body heading, with an angular deflection ϕ relative to the forward heading. Nares positions were given as:

$$x_{nL/nR} = x + \sqrt{\ell^2 + \left(\frac{d_{nares}}{2}\right)^2}\, cos\, (\theta + \phi \pm \gamma) \tag{n3}$$

$$y_{nL/nR} = y + \sqrt{\ell^2 + \left(\frac{d_{nares}}{2}\right)^2}\, sin\, (\theta + \phi \pm \gamma) \tag{n4}$$

with nose deflection bounded within $\pm\, \phi_{max}$ as dictated by mouse anatomy. The agent geometry is shown superimposed on a mouse body (Fig. 1D).

The independent motion of the nose is what allowed the agent to sample concentrations to the left and right of its current heading and adjust its heading toward higher concentrations (Fig. S1). The distribution of mouse nose deflections was approximately Gaussian. We therefore modeled the angular movement of the nose as an Ornstein-Uhlenbeck (OU) process, a mean-reverting

correlated random walk with a Gaussian stationary distribution. At each sniff, the nose deflection was updated according to:

$$\phi_t = \phi_{t-\Delta t} - \frac{\phi_{t-\Delta t}}{\tau}\Delta t + dW_t\sqrt{\frac{\Delta t}{\tau}} + k_{stereo}(c_L - c_R)\Delta t \quad \text{(n5)}$$

$$dW_t \sim N(0, \sigma_c^2) \quad \text{(n6)}$$

$$\sigma_c = \sigma_{min} + (\sigma_{max} - \sigma_{min})\frac{C_t}{k + C_t} \quad \text{(n7)}$$

where τ is the characteristic time constant of the process, σ_c is the concentration-dependent standard deviation of the nose deflection, dW_t is a normally distributed random variable with mean of zero and standard deviation σ_c, and k_{stereo} is the strength of the stereo-olfactory bias on nose movement (k=½). The concentration value C_t is the average concentration across both nares at time *t*:

$$C_t = \frac{(c_L + c_R)}{2} \quad \text{(n8)}$$

Here, c_L is the concentration at the left naris and c_R is the concentration at the right naris.
We observed that mouse speed increases with distance from the odor source (see Fig.3F). Because the agent in our model does not have information about its distance from the odor source, we used a concentration-dependent modulation of speed. Specifically, we use a Hill function with a cubic coefficient to approximate concentration-dependence of speed:

$$v_c = v_{max}\left(1 - \frac{C_t^3}{k^3 + C_t^3}\right) \quad \text{(n9)}$$

where v_{max} is the maximum velocity and k is ½.

Model Odor Environment. The agent must iteratively sample concentrations in an odor environment to navigate in the direction of higher concentration. To simulate the ambient concentration, *C(x,y),* we use a noisy bivariate exponential distribution normalized to a value of one at the source:

$$C(x,y) = max\left[e^{-\left(\frac{\sqrt{(x-x_{spot})^2 + (y-y_{spot})^2}}{2\,\sigma_{spot}^2}\right)}(1+\eta_t)\,, 0\right] \quad \text{(n10)}$$

$$\eta_t \sim U(-k_c, k_c) \quad \text{(n11)}$$

Here, (x_{spot}, y_{spot}) is the location of the source, σ_{spot} controls the width of the odor distribution around the source (model results were obtained with σ_{spot}=20 cm), and η_t is multiplicative uniform noise

added to each sniff to approximate the effect of turbulent flow, bounded at k_c=0.01. The concentration value at each sniff is also bounded such that it cannot take unrealistic negative values.

Concentration-Sensitive Model (CSM). The agent moves along forward heading θ at velocity v_c, iteratively sniffing the concentration at its nose coordinates (Eqns n1-n4). At each sniff, the agent's nose randomly samples to the left or right of the forward heading depending on the state of the random nose deflection process (Eqns n5-n7). It compares the current concentration sample, c_t, to the sample from the previous sniff, $c_{t-\Delta t}$. If c_t is greater than $c_{t-\Delta t}$, the agent sets its heading to the direction of the nose, $\theta_{t+\Delta t} := \theta_t + \phi_t$. If c_t is less than or equal to $c_{t-\Delta t}$, the agent turns away from the direction of the nose, $\theta_{t+\Delta t} := \theta_t - \phi_t$. This algorithm is effective at reproducing key parameters of mouse odor localization (Fig. 5A-F):

$$\theta_{t+\Delta t} = \theta_t + \phi_t \; if \; C_t > C_{t-\Delta t} \;\; else \; \theta_t - \phi_t \; if \; C_t \leq C_{t-\Delta t} \qquad \text{(n12)}$$

Correlated Random Walk (CRW) Controls. To test model behavior in the absence of odor-sensitivity, concentration-dependent turning was removed from the model and replaced by a random turning decision. Equation n12 is replaced by:

$$\theta_{t+\Delta t} = \theta_t + \phi_t \; if \; z > 0.5 \;\; else \; \theta_t - \phi_t \;\; z \sim U(0,1) \qquad \text{(n13)}$$

Reduced Model Controls. To evaluate the effects of different hypothesized features of mouse navigation, we constructed 8 model variant combinations by leaving out stereo-sniffing, concentration-dependent velocity, and/or concentration-dependent casting amplitude. We then evaluated the model performance in the absence of these features. To eliminate stereo-sniffing from the model, k_{stereo} in Equation n5 was set to zero. To remove concentration-dependent velocity from the model, Equation n9 was modified so that v_c was set equal to the constant v_{max}. To remove concentration-dependent casting amplitude from the model, Equation n7 was modified so that σ_c was set equal to the constant σ_{min}.

The same 8 reduced models were applied to the CRW controls, and results were averaged together to obtain control distributions.

RESULTS

A naturalistic open field odor-based spot-finding task was developed to study how mice find odor sources.

To examine the behaviors relevant to odor source localization, we designed a task that minimized non-olfactory cues. Five mice were trained to find a ~1.5 cm diameter circle of odorized wax within a rectangular behavioral arena in the dark (Fig. 1A). Odor sources for each of the trials (N=855) across all mice (N=5) were pseudo randomly distributed within the center of the testing table (Fig. 1B). Mice were placed in the arena and given 3 minutes to find the odor source. Mice were defined as having found the odor source if their nose position was within 1.5 cm of the center of the spot. An example trajectory shows the nose position of the mouse starting at the right-hand side of the arena and moving in a loop before successfully finding the spot (red circle; Fig. 1C). In this figure, the color indicates a measurement of curvature (see Methods) used to detect casting amplitude.

Agent-based models were developed to capture key aspects of mouse behavior discovered on the spot-finding task.

To explore the different mechanisms mice use for finding spots, we developed agent-based models that utilize concentration information in different ways. We describe two models, a concentration-sensitive model (CSM) and a correlated random walk (CRW) control model.

The basic geometry of both models consists of a 'body' point and a 'nose' point separated by a distance ℓ, where the nose is subdivided into a left and right sensor separated by an inter-nares distance d_{nares} (see Fig. 1D and Fig. S1 for model geometry). The model body moves at a given velocity v_c along a forward heading θ, changing the angular deflection its nose, ϕ, to the left or right according to a mean-reverting Ornstein-Uhlenbeck (OU) process.

The core of the CSM model is the temporal comparison of sniff-to-sniff concentration. At each discrete "sniff," it samples the odor at the position of its nose and compares the current odor concentration with the previously sampled concentration. If the current concentration is higher, the model "follows its nose" and aligns its forward heading θ with its nose (*i.e.,* $\theta := \theta + \phi$); if the current concentration is lower, its forward heading aligns in the opposite direction from the nose ($\theta := \theta - \phi$)

(eq n12). A normalized concentration gradient was modeled as a radially symmetric exponentially-decaying function (eq n10), and agents had no minimum threshold for concentration detection. A typical simulated nose trajectory showing a successful capture displays inter-sniff differences in odor concentration in arbitrary units (Fig.1E). The CSM model used here had parameters: Δt=0.1s, ℓ=5 cm, v_{max}=25cm, k=1/2, τ=0.1, σ_{min}=0.2, σ_{max}=0.3, and k_{stereo}=200 (defined in Methods). Further discussion of the concentration-dependent velocity (eq n9) and concentration-dependent casting amplitude (eq n7) components of the CSM below.

As a control, we introduce a CRW model that turns independently of concentration (eq n13). Rather, it aligns its heading with its nose 50% of the time and away from its nose 50% of the time, resulting in left and right turns in equal proportion. If mice are using directional odor cues to navigate, they should outperform the CRW. Eight different CRW models were tested, equivalent to the 8 model variants of the CSM model (see Fig. 5A). Note that some of these CRW models retain information about concentration in their velocities or casting amplitudes; however, as none of these parameters significantly influenced success rate, all 8 CRW models were combined into one control group.

Mice are successful at the open field odor-based spot-finding task, consistent with concentration sensitive models (CSM).

Mice were successful in 63% (N=537/855) trials when given 180 s to find the spot. While CRW control models had a similar success rate of ~60% when given 180 s, a closer look revealed that a more careful analysis was needed to compare models with data. After observing mice on videos, we determined they were not exploring the arena for the entire 180 s trial, while the CRW controls were continuously exploring the center of the arena (the decision rule for the agents at table boundaries was to bounce off like a billiard ball). We found the average time mice spent exploring the center of the arena to be only ~30 s and therefore ran the simulations for an equivalent 30 s to achieve a fair comparison. CRW controls with a maximum simulated time of 30 s were only successful in 20±4% (mean±s.d.) of trials, a statistically significant difference when compared to mice (63%) (Welch's t-test; p=21.96E-6, t-stat=11.35, df=6). The CSM successfully found the odor source on 95% of 1000 simulations within 30 s, significantly higher than the success rate of the CRW controls (95% vs. 20%; Welch's t-test, p=5.54E-20, t-stat 32.29, df=21; Fig. 2A). This is also

higher than success observed for the mice, but this is expected, as we did not attempt to model factors such as variable attention and motivation in mice which would only decrease success rate.

A logistic regression on successful versus unsuccessful trials for mouse data was performed, revealing several highly predictive explanatory variables (Table S1). Baited trials, in which a sliver of food was placed on the spot, had higher success rates (p=8.1E-16, β=1.98), potentially indicating higher motivation on these trials. Trials in which the mouse explored a greater percentage of the table overall predicted success (p=1.83E-6, β=3.91; see Fig. 2C). However, slower mice (p=1.68E-6, β=-0.21) were more successful, though they had faster average nose velocity (p=2.34E-5, β=0.21) and higher curvature (p=2.6E-10, β=6.06E-3), suggesting that slower forward body velocity and rapid lateral nose/head movements may be features of successful search strategies. Successful completion of this spot-finding task is thus dependent both on motivation and features of individual trajectories.

If mice are efficiently finding odor spots, we might expect them to quickly and directly navigate to the odor spot, thus exploring only a small fraction of the arena between their starting position and the odor spot. To measure table exploration, we divided the table into square bins of ~45 cm^2 (Fig. 2C, dashed vertical line). Mice explored an average of 33±17% (mean±s.d.) of the table before finding the spot. This estimate varied as a function of bin size and whether the odor source was found or not (Fig. 2C; two-way ANOVA interaction term; p<1E-100, F=69.41, df=97). Mice also explored progressively less of the table with increasing trial (ANOVA; p=4.92E-55, F=61.88, df=5) indicating that there is refinement of learning throughout the experiment.

Another potential measure of efficiency we looked at was the median time to find the spot during successful trials. We would expect mice navigating via scent to find the spot faster than CRW controls navigating via a random walk. The median time for mice to reach the spot was 13.2 s, while CRW controls took significantly longer (15.5 s) to reach the odor spot (Welch's t-test; p=5.25E-5, t-stat=4.07, df=6). In contrast, the CSM was much faster at performing the task (7.9 s) (Welch's t-test; p=3.78E-36, t-stat=13.21, df=794) (Fig. 2B).

A third measure of efficiency we examined was median nose displacement. We would expect CRW controls to have greater nose displacement than mice, as the model moves randomly around the table for 30 s. For mice, the total nose displacement through the center of the table on successful

trials had a median of 257 cm before successful spot localization, or ~6.3x the initial distance to the spot ‘as the crow flies.’ In contrast, the CRW controls’ median displacement was 709 cm, ~14x the minimum initial distance to the spot. This was greater than for successful trials of mice (Welch’s t-test; p=3.79E-89, t-stat=22.09, df=1053). The CSM was more efficient than both mouse and CRW controls, with median displacement of 169 cm, or 5x the initial distance to spot (mouse vs. CSM; Welch’s t-test; p=5.95E-10, tstat-6.25, df=1017).

Finally, we examined the survival function with respect to distance from the spot (Fig. 2D). Typically, a survival function is used to determine the probability that a variable of interest survives past some time point; here, we use it to describe the probability of mouse or model reaching a given distance away from the odor spot. For mice, there was a sharp increase in survival at the threshold distance of ~1.5 cm, with a more gradual increase toward 100% at about 90 cm from the odor spot (red line). Thus, mice on all trials successfully came within ~90 cm of the spot. CSM survival analysis revealed that nearly 100% of trials came within ~10 cm of the odor spots, drastically outperforming mice (magenta line). In contrast, CRW controls only reached ~20% success at the threshold distance of 1.5 cm, though they tended to reach intermediate minimum distances more frequently than mice (black line).

We conclude that mice find odor spots above chance levels established by the CRW controls. Mice and the CSM find spots faster than the CRW controls and have less nose deflection before finding spots. At a distance of ~1.5 cm, about the diameter of the odor spots, mice find the spots with greater accuracy than CRW controls, though the CSM outperforms them both.

Mouse behavior varies systematically as a function of distance from the odor source.

As suggested by the logistic regression analysis of mouse data, velocity and curvature are potentially important for successful navigation to an odor source. With minimal air currents in the room, the distribution of odor across the table is likely to be relatively static and decreasing with respect to the source. Mice therefore probably vary their behaviors reliably depending on their proximity to the odor source. When a mouse is far from the odor source, odor concentration will be low – possibly below the mouse’s odor detection threshold – though we are unable to evaluate this concern directly. As the mouse approaches the odor source, increasing odor cues may influence search strategy. We hypothesized that when within a critical distance from the odor source, mice

will locate the source with high probability, with increasing odor cues creating a so-called ‘basin of attraction’ within which mice would directly target the odor source. We conducted three analyses to test this hypothesis: 1) computing the percentage of time exploring at a given distance on a given trial (where was the mouse located?), and separately, the probability of finding the odor source as a function of distance given samples over all trials; 2) analyzing mouse heading relative to the odor source; and, 3) examining mouse velocity as a function of distance from the odor source.

First, we computed the percentage of total time mice spent at different distances from the odor source (Fig. 3A). We hypothesized that once a mouse detects the odor source, and until it reaches the food reward, it will avoid locations where it can no longer detect the odor. Specifically, we summed nose position in 50 concentric rings around the odor source at ~2 cm increments and divided by the total number of samples in each trial. This revealed an approximately uniform distribution across distance (red line). Doing the same analysis for the CRW control revealed an inverted-U shape (black line), suggesting that a random walk produces a stereotypical distribution of samples at intermediate distances from the spot. In contrast, the CSM produced an exaggerated (and fairly linear) increase in exploration as the agents approached the odor spot (magenta line). At a critical distance of ~10 cm from the odor source, occupancy levels during successful trials exceeded those expected from CRW control (Welch’s t-test; $p<1E-3$, t-stat 4.9, df=564).

To then compute the probability of finding the odor source in each ring, successful samples (samples when the spot was found) were divided by total samples (spot found + not found samples) (Fig. 3B). For mice, this resulted in a fairly flat distribution (red line), approaching 100% success more rapidly within ~10 cm. For the CSM, the probability of finding the odor source was consistently above the mice, and also fairly flat (magenta line). The CRW control was consistently below mice, but also increased within about ~10 cm to the source. This is likely due to some of the CRW model variants with concentration-dependent casting and velocity, to be described below.

Then, we examined mouse heading relative to the odor source for successful trials (Fig. 3C). If a mouse detects odor cues that provide insight into the location of the odor source, then the mouse’s nose should orient towards the source. At each position sample, the dot product between body-to-spot and body-to-nose vectors was computed. This value was divided by the magnitude of the vectors and the arccosine was then taken to obtain the angle of the nose relative to the spot. We found that orientation relative to the spot depends on distance from the odor spot (Watson-Williams

Test; p<1E-100, F=924.77, df=48), and has a median value not significantly different from zero within ~7.5 cm (circular test for equal medians with Bonferroni correction). The same analysis was performed with the CSM model (Fig. 3D), where it was again found that orientation relative to the spot depends on distance from the spot (Watson-Williams Test; p<1E-100, F=5.25, df=48).

Next, we examined mouse velocity as a function of distance from the odor source (Fig. 3E). We hypothesized that, as the mouse approached the odor source, it may reduce its running speed and/or average nose velocity to avoid running past or 'overshooting' the odor source. As mice approached the odor source during successful trials, nose velocity indeed slowed down (two-way ANOVA interaction term; p=1.2E-3, F=1.73, df=48), as did body velocity (two-way ANOVA interaction term; p=6.3E-4, F=1.79, df=48).

To model the observed effect of velocity decrease close to the odor spot, a concentration-dependent velocity term was implemented (eq n9). In this term, the maximum velocity, v_{max}, which was also derived from observations of mice, decreases with increasing concentration according to a cubic Hill function. This function was chosen as it was roughly linear and saturated at high concentrations.

In summary, we found that mice vary their search strategy and orient towards the spot as they approach it. Mice also slowed down as they approach the spot. Together, these behavioral changes potentially represent a speed-accuracy trade-off during the final stage of navigation towards an odor object, roughly within ~10 cm.

Casting increases near the odor spot and is modulated by velocity

Casting is seen in diverse circumstances ranging from plume navigation by moths to trail tracking by dogs; thus, mice may also cast during the open field odor-based spot-finding task. To measure casting amplitude, we calculated the $\log_{10}$ of the absolute value of the angular velocity of the nose divided by the linear velocity of the nose (Fig.1C; and see Methods). This is an appropriate measure for unsigned path curvature with units of (m^{-1}). We found that curvature increased as mice approached the odor source (ANOVA; p=1.21E-64, F=42, df=8), with an interaction between distance and successful versus unsuccessful trials (two-way ANOVA interaction term; p=3.9E-6, F=4.96, df=8), and within ~12 cm curvature for successful trials exceeded that of unsuccessful

trials (Welch's t-test, p=7.2E-5, t-stat=-4.26, df=61, Bonferroni correction), suggesting that curvature was higher close to the spot for successful trials. The average curvature for all trials (successful and unsuccessful) as a function of distance was well-fit by an exponential function ([a*exp(-b*x)+c]; R^2=0.73, a=0.42, b=0.15, c=-0.89).

To model the increase in curvature with approach to the spot, a concentration-dependent widening of the normal distribution was implemented (eq n7). Subsequent curvature analysis for the CSM and CRW control revealed that the simulations had systematically lower curvature for an unknown reason. Therefore, to compare with the mouse data, we z-scored the $\log_{10}$ of curvature within-session. CSM and CRW controls also showed increasing curvature as distance to the spot decreased, in general agreement with mouse data (Fig. 4C).

As curvature explicitly depended on inverse nose velocity (see Methods), we computed the distance between the nose and a line extending forward from the body heading as an alternate measure of casting (Fig. 4B). Using this alternate measure of nose deflection, we again found that casting increases as mice approach the odor source (ANOVA; p=1.0E-15, F=10.49, df=8), with an interaction between distance and successful versus unsuccessful trials (two-way ANOVA interaction term; p=0.011, F=2.47, df=8). However, we found no difference in successful versus unsuccessful trials within ~12 cm of the odor spot (Welch's t-test, p=0.13, t-stat=-1.50, df=68). The nose deflection of the CSM and CRW controls was in general agreement with mouse data, increasing near the odor spot (Fig. 4D).

Since velocity also decreased with decreasing distance to the odor spot, we performed additional analyses to see if we could separate the effects of velocity and distance on curvature and nose deflection. First, nose velocity and distance's effects on curvature did not interact (two-way ANOVA interaction term; p=0.8, F=0.77, df=32), but nose velocity (two-way ANOVA; p=2.8E-111, F=146, df=4) and distance (two-way ANOVA; p=2.9E-14, F=10.31, df=8) did have effects on curvature independently. To further analyze these effects, we did a stepwise linear regression analysis. The first step to include in the regression model was velocity (p=1.5E-151, F=803, t-stat=-28, β=-0.08, R^2=0.26), and the second was distance (p=3.35E-166, F=453, t-stat=-8.7, β=-0.015, R^2=0.28). We did the same analyses with the nose deflection measure. Again, there was no interaction between distance and velocity (two-way ANOVA interaction term; p=0.25, F=1.15, df=32), but there were individual effects of nose velocity (two-way ANOVA; p=1.19E-24, F=30.17, df=4) and distance

(two-way ANOVA; p=0.016, F=2.39, df=8). A stepwise regression analysis revealed that the first step to include in the model was velocity (p=3.82E-36, F=162, t-stat=-12.7, β=-0.07, R^2=0.05), while distance was the second step in the model (p=6.05E-35, F=80.83, t-stat=0.16, β=5E-4, R^2=0.05), though these effect sizes were weak. In summary, though there was no interaction between both measures of casting and velocity, individual effects of both variables made interpretation of results difficult. However, effect sizes of velocity were greater than those of distance, and velocity terms were included in the linear regression models first, suggesting casting and velocity are inter-related.

To assess whether animals began using non-odor cues to navigate towards the odor spots on later trials, we performed one-way ANOVAs on curvature and nose deflection at distances within ~12 cm for successful trials versus binned trial number (N=6). We did not find any effect of trial on curvature (ANOVA; p=0.91, F=0.3, df=5) or angular displacement (ANOVA; p=0.34, F=1.14, df=5), suggesting that casting close to the odor source was not affected by trial.

Overall, we find that casting amplitude of mice increases at distances close to the spot, suggesting that it may play a role in the successful navigation to a discrete odor object by mice. This change in casting is potentially correlated with velocity, which also decreases significantly during the approach to the spot.

Simulations reveal potential mechanisms driving behavior on the open field odor-based spot-finding task.

There are two possible mechanisms for odor source localization and trail following (Fig. 5A). Klinotaxis, or *serial-sniffing*, is the sequential sampling of odor at different locations and subsequent comparison. Tropotaxis, or *stereo-sniffing*, is a between-sensor comparison (e.g. inter-nostril in mammals) that provides sensory information on a much faster timescale than serial-sniffing, and does not require a memory trace of the odor. In both cases, the results of such comparisons can then be used to estimate the odor gradient at different spatial scales (cm-scale in klinotaxis and mm-scale in tropotaxis) and thus the direction to the source. Stereo-sniffing is a likely strategy employed by mice when odors travel across the nares at less than approximately 10 cm s^{-1} (Rajan et al., 2006) and may therefore be utilized during periods of pausing or low velocity

motion, or when the odor environment is relatively static. The interaction between serial-sniffing and stereo-sniffing behaviors during odor-source localization is unknown.

Simulations allow for further dissection of the odor-driven factors that impact behavior and successful odor source localization such as serial versus stereo sniffing. We created reduced CSMs to examine the relative contributions of three hypothesized behavioral components: stereo-sniffing, concentration-dependent velocity, and concentration-dependent casting amplitude. These model variants are denoted "-V" for the model lacking concentration-dependent velocity, "-S" for the model lacking stereo olfaction, "-C" for the model lacking concentration-dependent casting, "-VC", "-VS", "-SC" for models lacking multiple components, and "-VSC" for the model lacking all three components. While all reduced model variants outperformed CRW controls (Fig. 5B), removal of any of these behavioral components decreased model success. The removal of concentration-dependent velocity led to the largest change in success rate ('(-) V,' Δ34%), followed by stereo-sniffing ('(-) S,' Δ14%) and concentration-dependent casting amplitude ('(-) C,' Δ5%). The change in success rate was significant for removal of concentration-dependent velocity and stereo-sniffing, but not for concentration-dependent casting (one-way ANOVA, p=2.24E-82, F=100, df=8, multiple comparison test with Bonferroni correction). These behavioral components of olfactory search are synergistic; simultaneous removal of two or more of them leads to a greater reduction in success rate than the sum of reductions when components are removed individually. Model variant '(-) SC', in which both stereo-sniffing and concentration-dependent velocity are removed, resulted in a significant 26% change in model success (multiple comparison test with Bonferroni correction). All groups performed significantly better than the CRW Control, except for the reduced model with removal of all three terms ('(-) CSV').

Significance of model parameters was established by shuffling 6 parameters of the model 10k times, and comparing the effect of each parameter using a logistic regression (Table S2). All parameters (ℓ, v_{max}, d_{nares}, σ_{max}, σ_{min} and k_{stereo}) significantly impacted success rate in the ranges that were tested. To examine the effect of two parameters which are particularly important for stereo-sniffing, we plotted the average percent success as a function of d_{nares}, the distance between the two nostrils, and ℓ, the length between the body and the nose (Fig. 5C). Average success rate rapidly decreased as both d_{nares} and ℓ approached zero, but decreased more quickly with respect to ℓ, suggesting a relatively greater effect of body-nose length on success rate.

In summary, reduced models revealed that individual components of the overall strategy worked together to maximize task performance, with concentration-dependent velocity and stereo-sniffing having the greatest impact on successful task performance. Further analysis of model parameters revealed that body-nose length may have a greater contribution to effective stereo-sniffing than the distance between the two nostrils.

DISCUSSION

Here, we investigate the performance and navigation strategies of mice and a CSM on the open field odor-based spot-finding task and compare them to a CRW control model. We used a discrete, static target odor source to examine how olfactory-guided behavior changes as a function of distance from the odor source. Performance of mice exceeded that of the CRW control, indicating that mice were using odor cues to localize the odor target. Performance of the CSM exceeded that of mice, which we attribute to a lack of motivation to find the odor target or attention to the odor target in mice. However, this could also be a result of non-optimal sampling or a complex odor gradient, which was simply modeled as a stationary Gaussian distribution. Use of a discrete odor source allowed us to search for a basin of attraction where mice would reliably find odor sources. Our results suggest that, if this construct exists, it would be within 10cm from the odor source. We find that mice reliably orient towards the odor source from ~7.5 cm away, while decreasing their velocity, and increasing their casting amplitude at around the same distance. The CSM was built to capture these observations by using concentration-dependent velocity and casting terms. By removing components of the CSM, we were able to investigate potential mechanisms for spot-finding in mice. Removal of concentration-dependent velocity and stereo-sniffing terms had the greatest impact on performance. Varying the parameters of inter-nostril distance and neck length revealed that our model breaks down on insect-scale geometries but is otherwise robust across a wide range of geometries.

There is a potential speed-accuracy trade-off in search strategy close to the odor spot.

Creating reduced CSM models allowed us to examine the relative contributions of different strategies to successful odor source localization – a task that would be difficult to perform experimentally. We found that removal of concentration-dependent velocity led to the greatest single reduction in success rate (Δ25%). This suggests that reduced velocity at high concentrations

facilitates a “local” search near the odor source by causing the mouse to spend more time in regions of high concentration where it is more likely to hit its target. Providing further evidence for this, there was increased exploration time near the odor source for both mice and the CSM relative to the CRW control (Fig. 3A). Decreases in velocity close to the odor source also support this claim (Fig. 3C). We suggest that this phenomenon may be a type of speed-accuracy trade-off in spatial search behavior that deserves future study.

Stereo-sniffing facilitates search near the odor source.

During the task, mice slow down close to the source, perhaps because odor concentration during self-motion greater than velocities of 10 cm/s might result in airflow past the nostrils of greater than 10 cm/s, the threshold suggested for stereo-sniffing accuracy (Rajan et al., 2006). Stereo-sniffing allowed the model to preferentially cast in the direction of the odor source only when the odor gradient was large (i.e., near the source). Removal of stereo-sniffing led to a statistically significant decrease in model success (Δ11%), an observation compatible with the model put forward by Catania, 2013 (Catania, 2013), where stereo-sniffing becomes a relevant strategy on steep concentration gradients. The reduction in success when both concentration-dependent casting and stereo-sniffing were removed together (Δ23%) was greater than when each component was removed individually. This suggests that stereo-sniffing may help bias increased lateral search towards the direction of the source, allowing the nose to be “pulled” toward the source in relatively smooth arc-like trajectories.

Use of stereo-cues for navigation has also been observed in moles (Catania, 2013), snakes (Schwenk, 1994), and insects (Martin, 1965; Steck et al., 2010) suggesting it may be an evolutionarily conserved strategy. In mammals, neurons in the anterior olfactory nucleus may play a key role in integration of bilateral stimuli that are a key to stereo-sniffing (Kikuta et al., 2010) as this is one of the earliest locations in which information from both left and right naris can be integrated. We suggest that stereo-sniffing cues may play a pivotal role in fine discrimination of odor identity (Uchida and Mainen, 2003), as opposed to gross determination of odor source localization in space. Once a trail’s direction, or the rough direction to a spot is determined, stereo-sniffing cues may be useful for determining the direction to cast in order to continue following the direction of the trail (Khan et al., 2012), or steer towards the odor spot, as suggested here.

Future research may wish to consider whether there is a relationship between the physical distance between nostrils and the ‘effective’ nares separation of air drawn into the nasal cavity, or if the effective nares separation is determined by physical parameters such as inhalation volume, flux, and gradient. For example, inhalation in rats is largely from the lateral direction, rather than the front of the animal, as would be expected intuitively (Wilson and Sullivan, 1999). Pressure differences generated during sniffing inhalation at different magnitudes and frequencies (slow deep breath versus rapid sniffing) may also draw in relatively different concentrations of molecules from different distances away from the nares.

Serial-sniffing is related to general navigation strategies.

Navigation to an odor source with serial-sniffing is probably intimately tied to navigation through space using the cognitive map (Jacobs, 2012). We argue this because the distance traveled between the first to the second sniff in the concentration comparison needs to be factored in to determine an updated heading towards the source, or along the direction of the trail. In support of this view, hippocampal place cells may change their firing patterns (called remapping) to match the relocation of an orienting odor source in a circular arena (Zhang and Manahan-Vaughan, 2015). Recently, scent-marking as a tool for navigation and maintenance of a stable spatial map has been explored (Kulvicius et al., 2008; Lebedev et al., 2018). As we only analyzed the initial approaches to the odor spots, it is unlikely that scent marking was an issue in our experiment. Serial-sniffing can likely be generalized to trail finding behavior in dogs better than stereo-sniffing. Consider trying to determine the direction of a trail using stereo-sniffing: to optimize effectiveness, an animal would have to be oriented roughly perpendicular to the trail so that its nares are sensing maximally different concentrations. In contrast, studies with dogs repeatedly find that serial-sniffing of 2-5 footprints is required to determine a trail’s direction (Hepper and Wells, 2005; Thesen et al., 1993), a finding that is incompatible with determining trail direction with stereo-sniffing.

Casting is related to olfactory-guided navigation to a discrete, static odor source.

Casting has been observed at frequencies of ~4 Hz in moths flying upwind during pheromone-tracking (Charlton et al., 1993), and similar head-scanning behaviors have been observed in *Drosophila* larvae, rats, moles, and humans (Baker et al., 2018). In moths, casting has been reported to occur *outside* of an odor plume when a moth is attempting to re-acquire the odor

(Kennedy, 1983) and is characterized by loop-like flight trajectories (Kuenen and Cardé, 1994). In contrast, here we find that mouse casting, defined as either an increase in curvature or lateral head movement, increases during approach to the odor source. One potential explanation for this is that casting increases when there are intermittent gaps in the odor signal. However, if this were true, we would expect casting to be higher farther away from the odor source where the signal is lower; though, in support of this view, casting was modulated by velocity. We believe future experiments are necessary to determine the relationship between casting, velocity, and odor concentration in mice. While we did not find addition of concentration-dependent casting improves performance (Fig. 5A), we did not prove that this was true for all parameter sets in the CSM model. It is therefore conceivable that a set of parameters we did not test results in reduction in performance due to concentration-dependent casting.

Complexities to address in future studies include decision-rules and individual variability in strategy utilization.

Our data suggest that mice may use multiple search strategies during the navigation task, a finding previously shown in both fruit flies and ants. Draft et al., 2018 demonstrated that ants utilize a number of distinct antennal sampling strategies during trail following. Additionally, the relative contribution of strategies may also be variable between individuals, as has been observed during fruit fly navigation during odor presentation (Tao et al., 2018). A limitation of the current model is that it incorporates an ‘all or nothing’ decision at each sniff. It may be more appropriate to use a ‘softmax’ or other probabilistic decision rule to combine stereo- and serial-sniffing into a unified output. Also, a model where pausing emerges during epochs of uncertainty in sampling of the odor concentration gradient may be advantageous.

In summary, we discover that mice use multiple search strategies, including casting, during active navigation towards a discrete odor object, modulating features of behavior as a function of distance from the target. A concentration-sensitive model successfully recapitulates mouse behavior, while allowing for the analysis of the relative contributions of stereo-sniffing, concentration-dependent velocity, and concentration-dependent casting amplitude. Future work is needed to experimentally dissect how these variables impact mouse navigation and whether additional parameters are important in successful navigation to a static odor source.

ACKNOWLEDGEMENTS

We thank Gregory LaRocca for technical help and members of the Urban laboratory as well as Yu Chen and Dr. Robert Kass for helpful discussions. We thank Kathy Nagel and Jonathan Victor for helpful comments on the manuscript. Special thanks to Peter Jones for designing and building the behavior table used in this experiment.

COMPETING INTERESTS

The authors declare no competing financial interests.

FUNDING

This work was supported by the National Science Foundation [1555862 to N.N.U., 1555916 to B.E.]; the National Institutes of Health, National Institute on Deafness and Other Communication Disorders [F30DC015161 to A.L.], and the Pennsylvania Department of Health's Commonwealth Universal Research Enhancement Program [N.N.U.].

FIGURE CAPTIONS

Figure 1. Experimental setup and methods. A) The open field odor-based spot-finding task for testing olfactory search behavior in mice is a 45" x 36" (1.143 m x 0.9144 m) table made from three layers of plexiglass, designed to allow an infrared (IR) camera to view the mice from below. An odor spot was placed pseudo randomly on the table by the experimenter before starting the trial, either unbaited or baited with a chocolate or peanut reward. Then the mouse was placed on the right-hand side of the table and allowed to freely explore the arena. **B)** The pseudorandom odor spot distribution for all trials (N=853; trials where spot is less than 4 cm from the edge are excluded). **C)** A typical example trajectory where the mouse finds the odor spot, showing nose tracking with the casting measure (unsigned curvature) on the color axis. The mouse is placed in the middle of the right side of the table and takes a meandering trajectory towards the nearest wall. Then, the mouse begins to hone in on the odor spot (red circle). **D)** Model specification of the body position (x,y), and the body angle θ (red). The nose position (x_n,y_n) is the mean position between the left and right nares, nose angle ϕ (dark blue) is the angle between θ and nose position, and the head-body length ℓ is the distance between the body position and the nose position (note that nose position is sub-divided into two nostrils, separated by a distance d_{nares}). **E)** A sample simulated nose trajectory of the CSM where the agent starts at the middle-right side of the simulated arena

and works its way over to the left side, successfully finding the spot, indicated by the nose crossing the 2 cm capture radius (red circle). Color indicates the difference in concentration between two consecutive sniffs.

Figure 2. Mice and the CSM efficiently locate the odor source. A) Mean percentage of correct trials for mice (N=5) compared to control correlated random walk (CRW) simulations (N=8) and concentration-dependent simulations (N=64). Mice are successful on 65% of trials, while CRW controls find the spot 27% of the time, significantly lower than mice (Welch's t-test; p=21.96E-6, t-stat=11.35, df=6). The concentration-sensitive model (CSM) finds the spot 95% of the time. (x=median, dots=individual animals or simulations) **B)** Mouse exploration time before finding the odor spot was compared to the model time to find the spot. The mean time it took mice to find the spot was about 30 s. However, the median exploration time (time exploring the center of the table excluding 4 cm from the edges) before finding the spot was even lower, ~13 s, and this exploration time was comparable to models' total time to find the spot. Here, the total time for models and exploration time for mice are plotted (circle=mean, x=median, dots=individual trials). The CSM median time to spot was 7.9 s, faster than mice; in contrast, the CRW controls (black) took ~16 s to find the spot, significantly greater than mice (Welch's t-test; p=5.25E-5, t-stat=4.07, df=6). **C)** To analyze exploration of the table, the table was broken up into N equal area bins from ~0.9 cm^2 to ~980 cm^2 and the percentage of table explored was calculated for each bin size. Independent of bin size, mice explored a greater percentage of the table during successful trials (red line=mean±s.e.m.) compared to unsuccessful trials (blue line=mean±s.e.m.) (two-way ANOVA interaction term; p<1E-100, F=69.41, df=97). **D)** Survival function for minimum distance from the odor spot for mice, CSM and CRW. Mice on all trials successfully came within ~90 cm of the spot and were dramatically outperformed by CSM simulations, of which nearly 100% reached ~10 cm of the odor spots. In contrast, only 70% of CRW controls reached ~10 cm of the spot.

Figure 3. Mouse behavior varies systematically as mice approach the odor source. A) 50 concentric rings spaced at ~2 cm were defined around each odor spot. The number of samples in each ring divided by the total number of samples in a trial was computed. During successful trials, percent sampled increased or remained steady as mice approached the odor spot (red line=mean±s.e.m.). In contrast for the CRW control, percent sampled decreased near the spot (black line=mean±s.e.m.). For the CSM, percent sampled increased steadily with decreasing

distance (magenta line=mean±s.e.m.). **B)** The probability of finding the spot was computed as counts in each ring for successful trials divided by total counts over all trials. Mice tended to do better than the CRW controls at all distances (<=100 cm) from the odor spot, nearly the entire length of the table. Similarly, the CSM qualitatively outperformed mice across the entire length of the table. **C)** The orientation of the nose relative to the spot was computed using the arccosine of the normalized dot product between the vectors from body-to-spot and body-to-nose. Then, the angle was binned based on distance from the spot, and normalized by total counts in each distance bin. With this measure, angles of 0° indicate alignment of the nose with the odor spot. A significant increase in alignment with the spot was observed within ~10 cm of the spot (Watson-Williams Test; p<1E-100, F=924.77, df=48). **D)** Orientation of the nose relative to the spot for the CSM model shows the CSM model aligning with the odor spot at distances farther out than the mice. **E)** The nose velocity versus distance was computed and averaged across trials separately for successful (red line=mean±s.e.m.) and unsuccessful (blue line=mean±s.e.m.) trials. As mice approach the odor spot on successful trials, they tend to slow down (two-way ANOVA interaction term; p=1.2E-3, F=1.73, df=48). **F)** The nose velocity for CSM (magenta line) and CRW controls (black line) was modeled as a decay with respect to concentration, capturing the observed decrease in velocity close to the odor spot.

Figure 4. Analysis of casting amplitude in mice and CSM using curvature and nose deflection measures. A) Unsigned curvature of the nose was computed as a measure of casting amplitude (see Methods) and averaged across successful trials (red line=mean±s.e.m.). Casting increased as mice approached the odor spot (ANOVA; p=1.21E-64, F=42, df=8), and was significantly higher on successful trials within ~12 cm compared to unsuccessful trials (Welch's t-test, p=7.2E-5, t-stat=-4.26, df=61, Bonferroni correction). **B)** Unsigned curvature of the nose for the CSM and CRW controls was computed. For both models, casting amplitude increased as the spot was approached, though the increase for the CSM was greater. **C)** As an alternative measure of casting, the absolute angular deflection of the nose from midline was calculated by drawing a line forward from the body in the direction of the velocity vector and computing the distance from the nose to that line. Using this measure of nose deflection, casting amplitude also increased close to the odor spot (ANOVA; p=1.0E-15, F=10.49, df=8). **D)** The nose deflection of the CSM and CRW control was in general agreement with mice.

Figure 5. Reduced versions of the CSM reveal the importance of concentration-dependent velocity and stereo-sniffing. A) Schematic depicting serial-sniffing and stereo-sniffing. Serial-sniffing involves comparison of odor samples "A" and "B" with a difference in odor concentration ΔC_{AB} over time Δt, which is related to the mouse velocity between samples. Stereo-sniffing involves the rapid inter-nares comparison of odor samples "a" and "b", across a much smaller sample-to-sample distance than in serial-sniffing. **B)** Reduced concentration-dependent models (magenta=CSM, blue=CSM with removed components) and CRW controls (gray). Eight variants of the CSM were tested. Nomenclature as follows. '(-) C': concentration-dependent casting was removed by setting $\sigma_c = \sigma_{min}$; (-) S: stereo-sniffing was removed by setting k_{stereo}=0; '(-) V': concentration-dependent velocity was removed by setting v=v_{max}. Thus, '(-) VSC' denotes the model where all three components are removed. Removal of concentration-dependent velocity '(-)V' resulted in the largest decrease in performance. Removal of both concentration-dependent velocity and stereo-sniffing '(-) VS' reduced performance additively with respect to each component individually. Magenta '*' denote statistically significant comparison with the CSM, while the blue '#' denotes a statistically significant difference between '(-) VS' when compared with both the '(-)V' and '(-)S' separately. The eighth bar, '(-)VSC' has none of the concentration-dependent components, but remains concentration-sensitive in principle. However, performance of the '(-)VSC' model was not significantly different from that of the 8 CRW controls (gray) (denoted with gray 'n.s.'). Note that the same 8 'reduced' variants of the CRW were used, but were combined into one control group, as there were no differences between groups. **C)** To investigate parameters that significantly affected success rate in the CSM model, 10k simulations were performed using random combinations of parameters across a limited range of values. Significant variables included the inter-nares distance, d_{nares}, and the neck length, ℓ. Success rate dropped off rapidly when either of these two parameters was decreased.

SUPPLEMENTAL CAPTIONS

Figure S1. Detailed model geometry. A) Model specification of the body position (x,y), and the body angle θ. The nose position (x_n,y_n) is the mean position between the left and right nares. **B)** Nose angle ϕ (dark blue) is the angle between θ and nose position. **C)** The head-body length ℓ is the distance between the body position and the nose position (note that nose position is sub-divided into two nostrils, separated by a distance d_{nares}).

Table S1. Logistic regression analysis on spot-finding success in mice. Significant variables in bold.

Table S2. Logistic regression analysis of CSM parameters on spot-finding success. Significance and value ranges of each parameter are listed.

ABBREVIATIONS

CSM – concentration-sensitive model

CRW – correlated random walk

OU – Ornstein-Uhlenbeck

Δt – change in time (s)

ℓ – nose-to-body length parameter (cm)

v_{max} – maximum velocity parameter (cm/s)

k – concentration-dependent parameter

σ_{min} – concentration-dependent parameter

σ_{max} – concentration-dependent parameter

k_{stereo} – stereo-olfaction parameter

d_{nares} – inter-nostril parameter (cm)

ANOVA – Analysis Of VAriance

LED – light emitting diode

dPhi/nV – numerical derivative of the arctangent of angular nose velocity that is then divided by linear nose velocity

x' – derivative (of x)

x_n – nose coordinate

θ – heading of model body (degrees)

φ – heading of model nose relative to body (degrees)

C_t – concentration magnitude (A.U.)

η_t – multiplicative uniform noise

(-)C – CSM model without concentration-dependent casting, $\sigma = \sigma_{min}$

(-)S – CSM model without stereo-sniffing component, $k_{stereo}=0$

(-)V – CSM model without concentration-dependent velocity, $v=v_{max}$

IR – infrared

REFERENCES

Baker, K.L., Dickinson, M., Findley, T.M., Gire, D.H., Louis, M., Suver, M.P., Verhagen, J.V., Nagel, K.I., Smear, M.C., 2018. Algorithms for Olfactory Search across Species. J. Neurosci. 38, 9383–9389. https://doi.org/10.1523/JNEUROSCI.1668-18.2018

Ben-Shaul, Y., 2017. OptiMouse: a comprehensive open source program for reliable detection and analysis of mouse body and nose positions. BMC Biol. 15, 41. https://doi.org/10.1186/s12915-017-0377-3

Bhattacharyya, U., Bhalla, U.S., 2015. Robust and rapid air-borne odor tracking without casting. eNeuro 2, ENEURO–0102.

Budick, S.A., Dickinson, M.H., 2006. Free-flight responses of Drosophila melanogaster to attractive odors. J. Exp. Biol. 209, 3001–3017. https://doi.org/10.1242/jeb.02305

Cardé, R.T., Willis, M.A., 2008. Navigational Strategies Used by Insects to Find Distant, Wind-Borne Sources of Odor. J. Chem. Ecol. 34, 854–866. https://doi.org/10.1007/s10886-008-9484-5

Catania, K.C., 2013. Stereo and serial sniffing guide navigation to an odour source in a mammal. Nat. Commun. 4, 1441. https://doi.org/10.1038/ncomms2444

Charlton, R.E., Kanno, H., Collins, R.D., Carde, R.T., 1993. Influence of pheromone concentration and ambient temperature on flight of the gypsy moth, Lymantria dispar (L), in a sustained-flight wind tunnel. Physiol. Entomol. 18, 349–362.

Draft, R.W., McGill, M.R., Kapoor, V., Murthy, V.N., 2018. Carpenter ants use diverse antennae sampling strategies to track odor trails. J. Exp. Biol. 221, jeb185124. https://doi.org/10.1242/jeb.185124

Gire, D.H., Kapoor, V., Arrighi-Allisan, A., Seminara, A., Murthy, V.N., 2016. Mice Develop Efficient Strategies for Foraging and Navigation Using Complex Natural Stimuli. Curr. Biol. 0. https://doi.org/10.1016/j.cub.2016.03.040

Hangartner, W., 1969. Structure and variability of the individual odor trail in Solenopsis geminata Fabr. (Hymenoptera, Formicidae). J. Comp. Physiol. 62, 111–120. https://doi.org/http://dx.doi.org/10.1007/BF00298046

Hepper, P.G., Wells, D.L., 2005. How Many Footsteps Do Dogs Need to Determine the Direction of an Odour Trail? Chem. Senses 30, 291–298. https://doi.org/10.1093/chemse/bji023

Hills, T.T., Todd, P.M., Lazer, D., Redish, A.D., Couzin, I.D., 2015. Exploration versus exploitation in space, mind, and society. Trends Cogn. Sci. 19, 46–54. https://doi.org/10.1016/j.tics.2014.10.004

Jacobs, L.F., 2012. From chemotaxis to the cognitive map: The function of olfaction. Proc. Natl. Acad. Sci. 109, 10693–10700. https://doi.org/10.1073/pnas.1201880109

Janabi-Sharifi, F., Hayward, V., Chen, C.S.J., 2011. Discrete-time adaptive windowing for velocity estimation. IEEE Trans. Control Syst. Technol.

Jones, P., Urban, N.N., 2018. Mice follow odor trails using stereo olfactory cues and rapid sniff to sniff comparisons. bioRxiv.

Kennedy, J.S., 1983. Zigzagging and casting as a programmed response to wind-borne odour: a review. Physiol. Entomol. 8, 109–120. https://doi.org/10.1111/j.1365-3032.1983.tb00340.x

Khan, A.G., Sarangi, M., Bhalla, U.S., 2012. Rats track odour trails accurately using a multi-layered strategy with near-optimal sampling. Nat. Commun. 3, 703. https://doi.org/10.1038/ncomms1712

Kikuta, S., Sato, K., Kashiwadani, H., Tsunoda, K., Yamasoba, T., Mori, K., 2010. Neurons in the anterior olfactory nucleus pars externa detect right or left localization of odor sources. Proc. Natl. Acad. Sci. 107, 12363–12368. https://doi.org/10.1073/pnas.1003999107

Koehl, M.A.R., Koseff, J.R., Crimaldi, J.P., McCay, M.G., Cooper, T., Wiley, M.B., Moore, P.A., 1995. Filtering of Information in an Odor Plume. Mol Cell Neurosci 6, 544.

Kuenen, L.P.S., Cardé, R.T., 1994. Strategies for recontacting a lost pheromone plume: casting and upwind flight in the male gypsy moth. Physiol. Entomol. 19, 15–29. https://doi.org/10.1111/j.1365-3032.1994.tb01069.x

Kulvicius, T., Tamosiunaite, M., Ainge, J., Dudchenko, P., Wörgötter, F., 2008. Odor supported place cell model and goal navigation in rodents. J. Comput. Neurosci. 25, 481–500. https://doi.org/10.1007/s10827-008-0090-x

Lebedev, M.A., Pimashkin, A., Ossadtchi, A., 2018. Navigation Patterns and Scent Marking: Underappreciated Contributors to Hippocampal and Entorhinal Spatial Representations? Front. Behav. Neurosci. 12. https://doi.org/10.3389/fnbeh.2018.00098

Manurung, A., 2016. Numerical methods for velocity estimation - File Exchange - MATLAB Central [WWW Document]. URL http://www.mathworks.com/matlabcentral/fileexchange/52381-numerical-methods-for-velocity-estimation (accessed 9.4.17).

Marsh, D., Kennedy, J.S., Ludlow, A.R., 1978. An analysis of anemotactic zigzagging flight in male moths stimulated by pheromone. Physiol. Entomol. 3, 221–240. https://doi.org/10.1111/j.1365-3032.1978.tb00152.x

Martin, H., 1965. Osmotropotaxis in the Honey-Bee. Nature 208, 59–63. https://doi.org/10.1038/208059a0

Means, L.W., Alexander, S.R., O'Neal, M.F., 1992. Those cheating rats: male and female rats use odor trails in a water-escape "working memory" task. Behav. Neural Biol. 58, 144–151.

Papale, A.E., Stott, J.J., Powell, N.J., Regier, P.S., Redish, A.D., 2012. Interactions between deliberation and delay-discounting in rats. Cogn. Affect. Behav. Neurosci. 12, 513–526. https://doi.org/10.3758/s13415-012-0097-7

Pierce-Shimomura, J.T., Morse, T.M., Lockery, S.R., 1999. The fundamental role of pirouettes in Caenorhabditis elegans chemotaxis. J. Neurosci. 19, 9557–9569.

Porter, J., Craven, B., Khan, R.M., Chang, S.-J., Kang, I., Judkewicz, B., Volpe, J., Settles, G., Sobel, N., 2007. Mechanisms of scent-tracking in humans. Nat. Neurosci. 10, 27–29. https://doi.org/10.1038/nn1819

Rajan, R., Clement, J.P., Bhalla, U.S., 2006. Rats smell in stereo. Science 311, 666–670. https://doi.org/10.1126/science.1121054

Schwenk, K., 1994. Why Snakes Have Forked Tongues. Science 263, 1573–1577. https://doi.org/10.1126/science.263.5153.1573

Steck, K., Knaden, M., Hansson, B.S., 2010. Do desert ants smell the scenery in stereo? Anim. Behav. 79, 939–945. https://doi.org/10.1016/j.anbehav.2010.01.011

Tao, L., Ozarkar, S., Bhandawat, V., 2018. Statistical structure of locomotion and its modulation by odors. bioRxiv 404772.

Thesen, A., Steen, J.B., Doving, K.B., 1993. Behaviour of dogs during olfactory tracking. J. Exp. Biol. 180, 247–251.

Uchida, N., Mainen, Z.F., 2003. Speed and accuracy of olfactory discrimination in the rat. Nat. Neurosci. 6, 1224–1229.

Vickers, N.J., 2000. Mechanisms of animal navigation in odor plumes. Biol. Bull. 198, 203–212.

Wallace, D.G., Gorny, B., Whishaw, I.Q., 2002. Rats can track odors, other rats, and themselves: implications for the study of spatial behavior. Behav. Brain Res. 131, 185–192.

Wesson, D.W., Donahou, T.N., Johnson, M.O., Wachowiak, M., 2008. Sniffing Behavior of Mice during Performance in Odor-Guided Tasks. Chem. Senses 33, 581–596. https://doi.org/10.1093/chemse/bjn029

Willis, M.A., Avondet, J.L., Finnell, A.S., 2008. Effects of altering flow and odor information on plume tracking behavior in walking cockroaches, Periplaneta americana (L.). J. Exp. Biol. 211, 2317–2326. https://doi.org/10.1242/jeb.016006

Wilson, D.A., Sullivan, R.M., 1999. Respiratory Airflow Pattern at the Rat's Snout and an Hypothesis Regarding Its Role in Olfaction. Physiol. Behav. 66, 41–44. https://doi.org/10.1016/S0031-9384(98)00269-8

Zhang, S., Manahan-Vaughan, D., 2015. Spatial Olfactory Learning Contributes to Place Field Formation in the Hippocampus. Cereb. Cortex 25, 423–432. https://doi.org/10.1093/cercor/bht239

1043 **FIGURE 1**

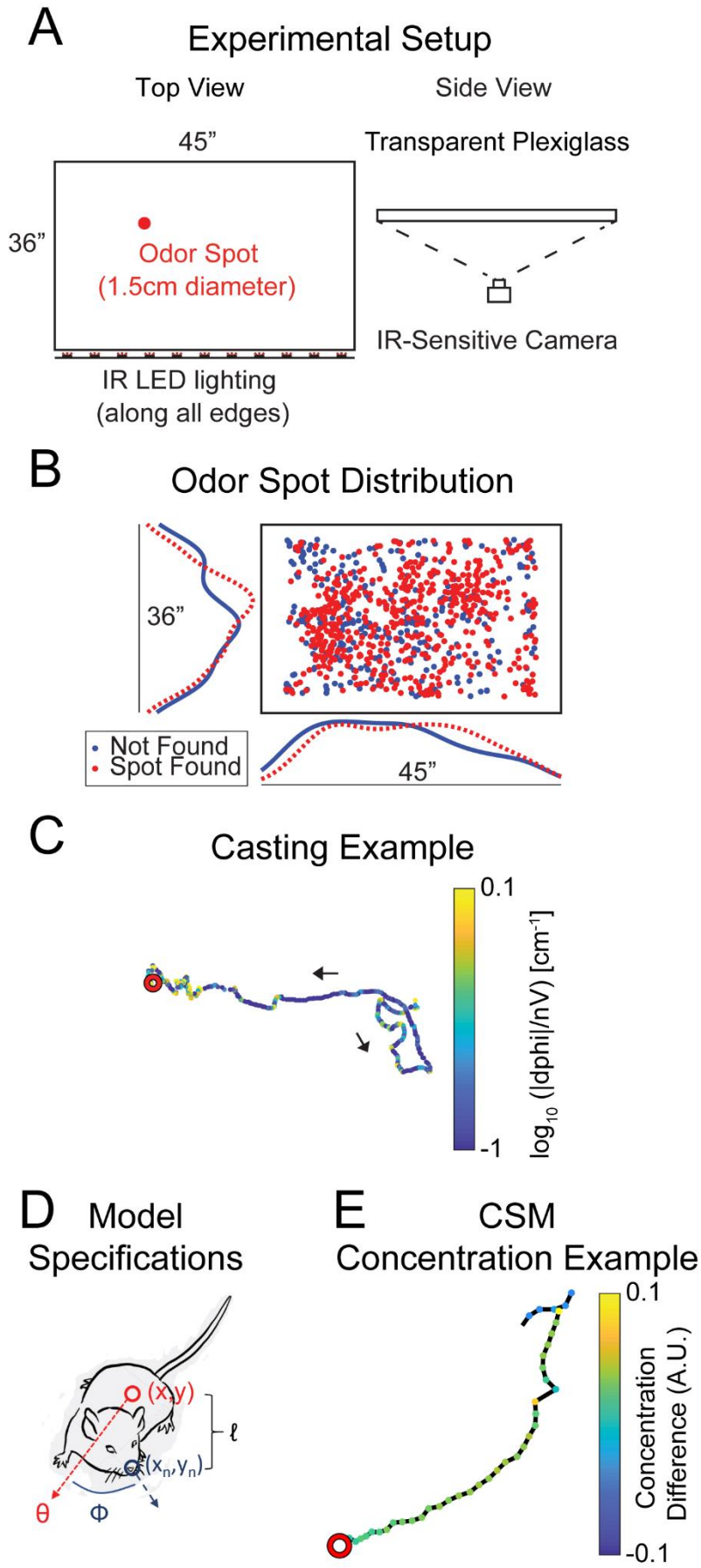
A
Experimental Setup
Top View
Side View
45”
Transparent Plexiglass
36”
Odor Spot
(1.5cm diameter)
IR-Sensitive Camera
IR LED lighting
(along all edges)
B
Odor Spot Distribution
36”
Not Found
Spot Found
45”
C
Casting Example
0.1
-1
log10 (|dphi|/nV) [cm-1]
D
Model
Specifications
(x,y)
ℓ
(xn,yn)
θ
Φ
E
CSM
Concentration Example
0.1
-0.1
Concentration
Difference (A.U.)

1044

1045 **FIGURE 2**

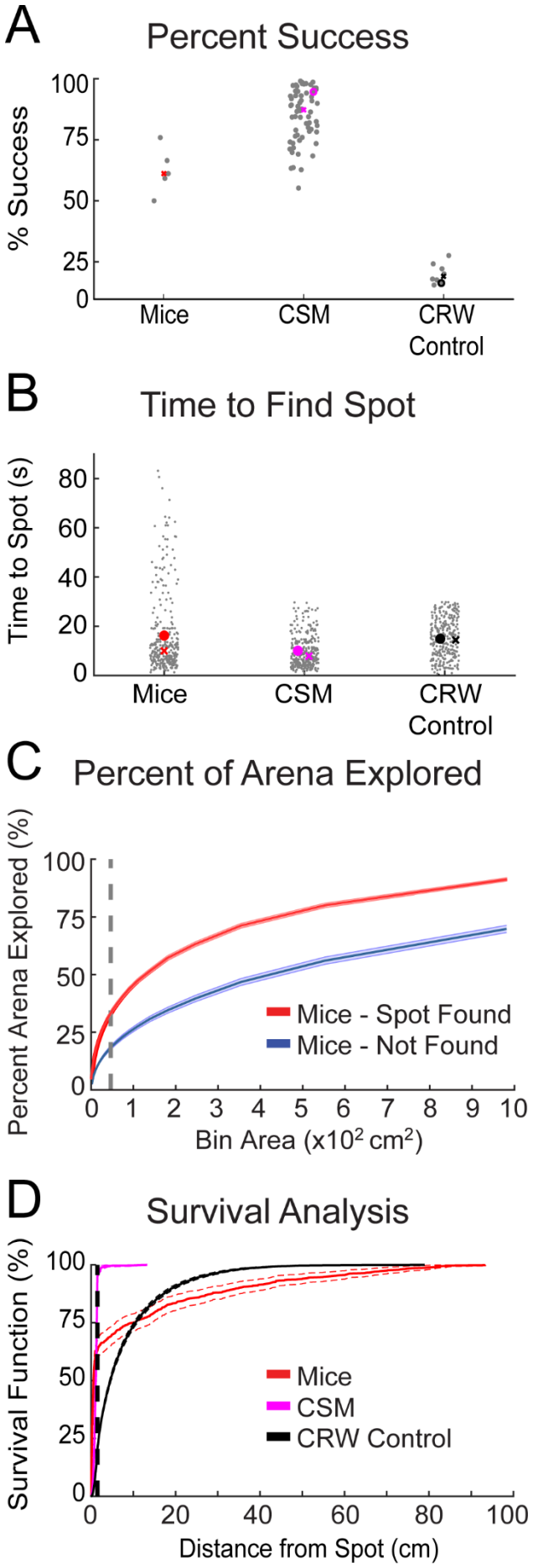
A
Percent Success
% Success
100
75
50
25
0
Mice
CSM
CRW Control
B
Time to Find Spot
Time to Spot (s)
80
60
40
20
0
Mice
CSM
CRW Control
C
Percent of Arena Explored
Percent Arena Explored (%)
100
75
50
25
0
0 1 2 3 4 5 6 7 8 9 10
Bin Area (x10² cm²)
Mice - Spot Found
Mice - Not Found
D
Survival Analysis
Survival Function (%)
100
75
50
25
0
0 20 40 60 80 100
Distance from Spot (cm)
Mice
CSM
CRW Control

1046

FIGURE 3

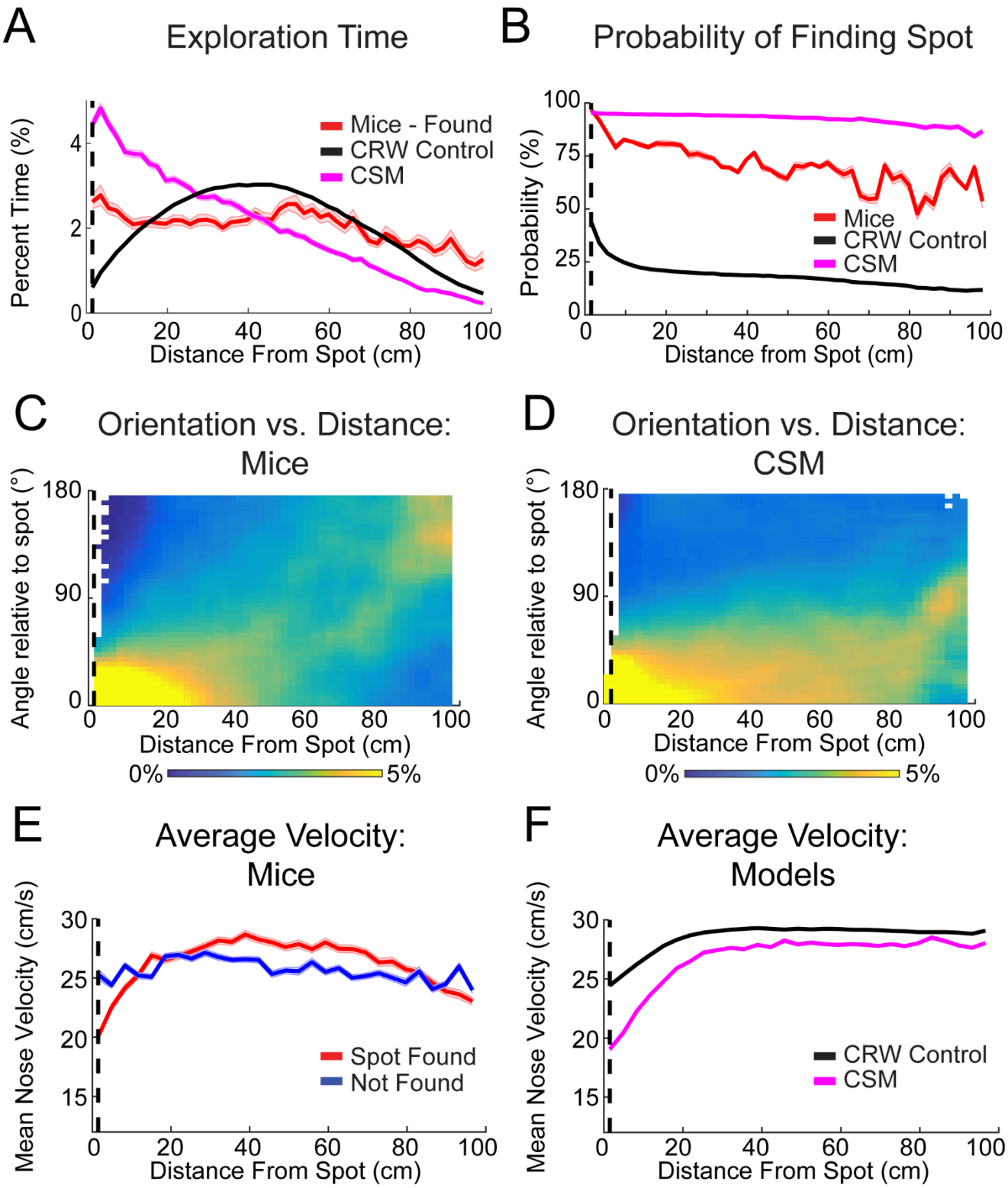
A
Exploration Time
Percent Time (%)
Distance From Spot (cm)
Mice - Found
CRW Control
CSM
B
Probability of Finding Spot
Probability (%)
Distance from Spot (cm)
Mice
CRW Control
CSM
C
Orientation vs. Distance: Mice
Angle relative to spot (°)
Distance From Spot (cm)
0%
5%
D
Orientation vs. Distance: CSM
Angle relative to spot (°)
Distance From Spot (cm)
0%
5%
E
Average Velocity: Mice
Mean Nose Velocity (cm/s)
Distance From Spot (cm)
Spot Found
Not Found
F
Average Velocity: Models
Mean Nose Velocity (cm/s)
Distance From Spot (cm)
CRW Control
CSM

FIGURE 4

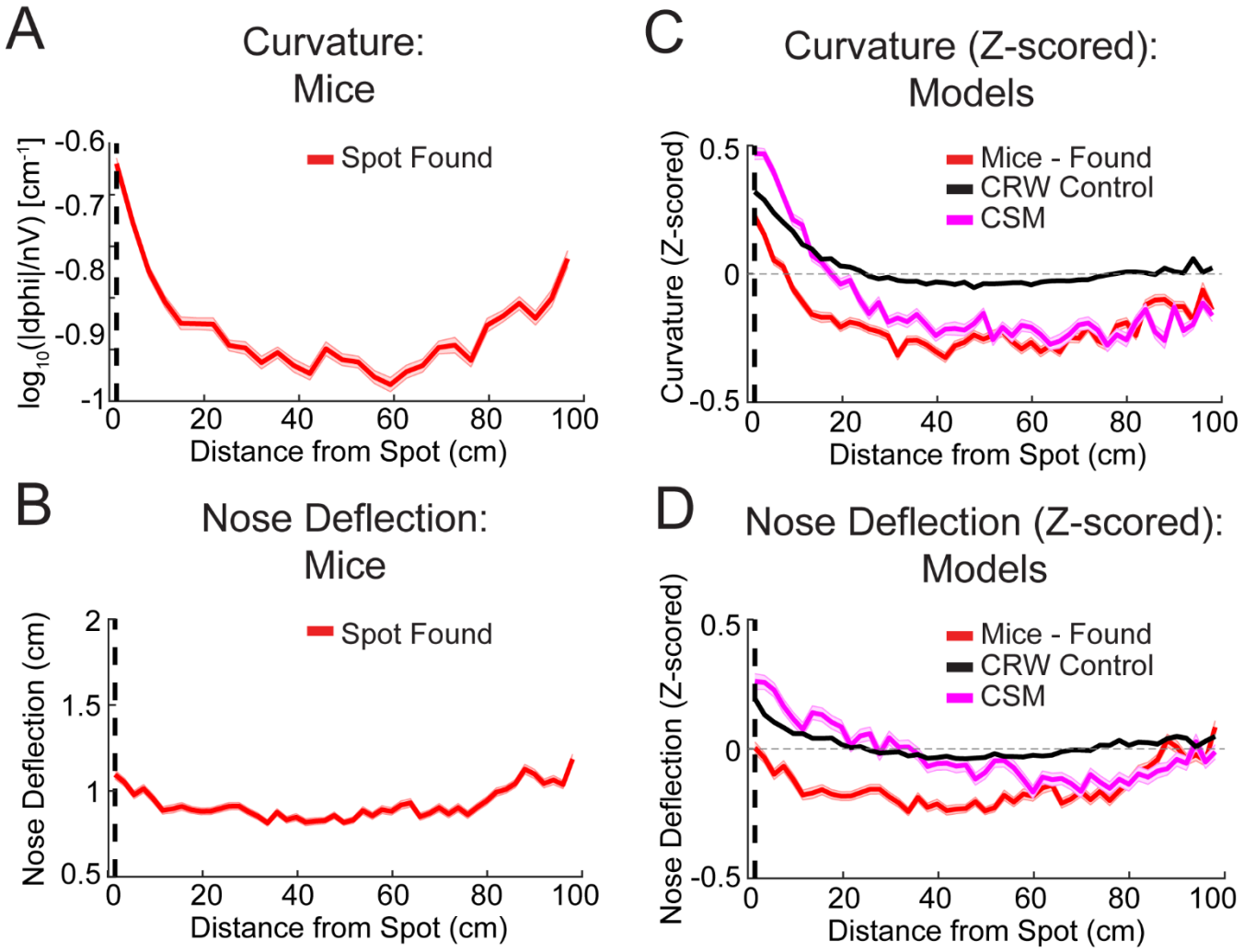
A
Curvature:
Mice
Spot Found
log10(|dphi|/nV) [cm-1]
-0.6
-0.7
-0.8
-0.9
-1
0
20
40
60
80
100
Distance from Spot (cm)
B
Nose Deflection:
Mice
Spot Found
Nose Deflection (cm)
2
1.5
1
0.5
0
20
40
60
80
100
Distance from Spot (cm)
C
Curvature (Z-scored):
Models
Mice - Found
CRW Control
CSM
Curvature (Z-scored)
0.5
0
-0.5
0
20
40
60
80
100
Distance from Spot (cm)
D
Nose Deflection (Z-scored):
Models
Mice - Found
CRW Control
CSM
Nose Deflection (Z-scored)
0.5
0
-0.5
0
20
40
60
80
100
Distance from Spot (cm)

FIGURE 5

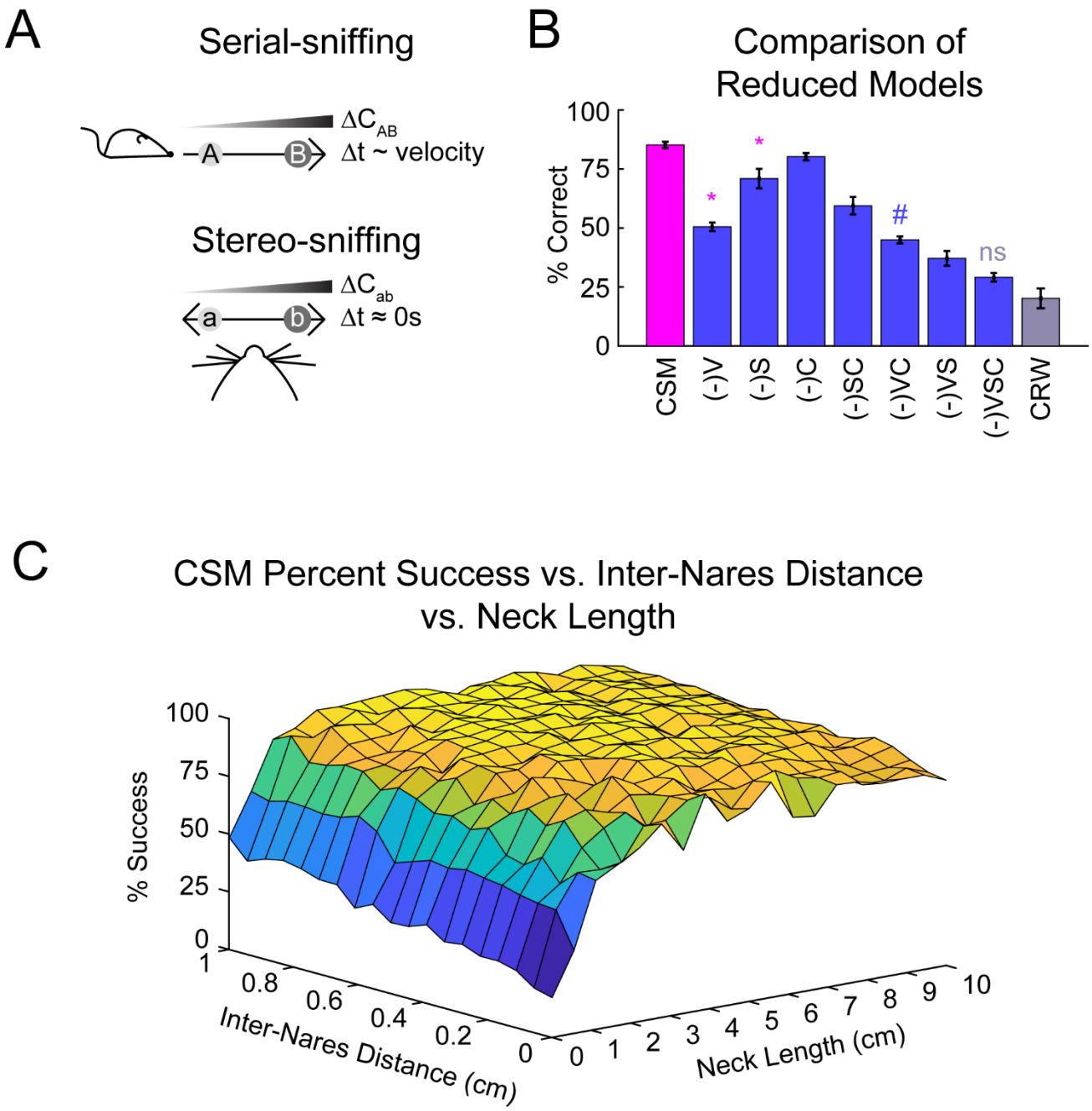
A
Serial-sniffing
ΔC_AB
A
B
Δt ~ velocity
Stereo-sniffing
ΔC_ab
a
b
Δt ≈ 0s
B
Comparison of Reduced Models
% Correct
100
75
50
25
0
*
*
#
ns
CSM
(-)V
(-)S
(-)C
(-)SC
(-)VC
(-)VS
(-)VSC
CRW
C
CSM Percent Success vs. Inter-Nares Distance vs. Neck Length
% Success
100
75
50
25
0
1
0.8
0.6
0.4
0.2
0
Inter-Nares Distance (cm)
0
1
2
3
4
5
6
7
8
9
10
Neck Length (cm)

SUPPLEMENTAL FIGURE 1

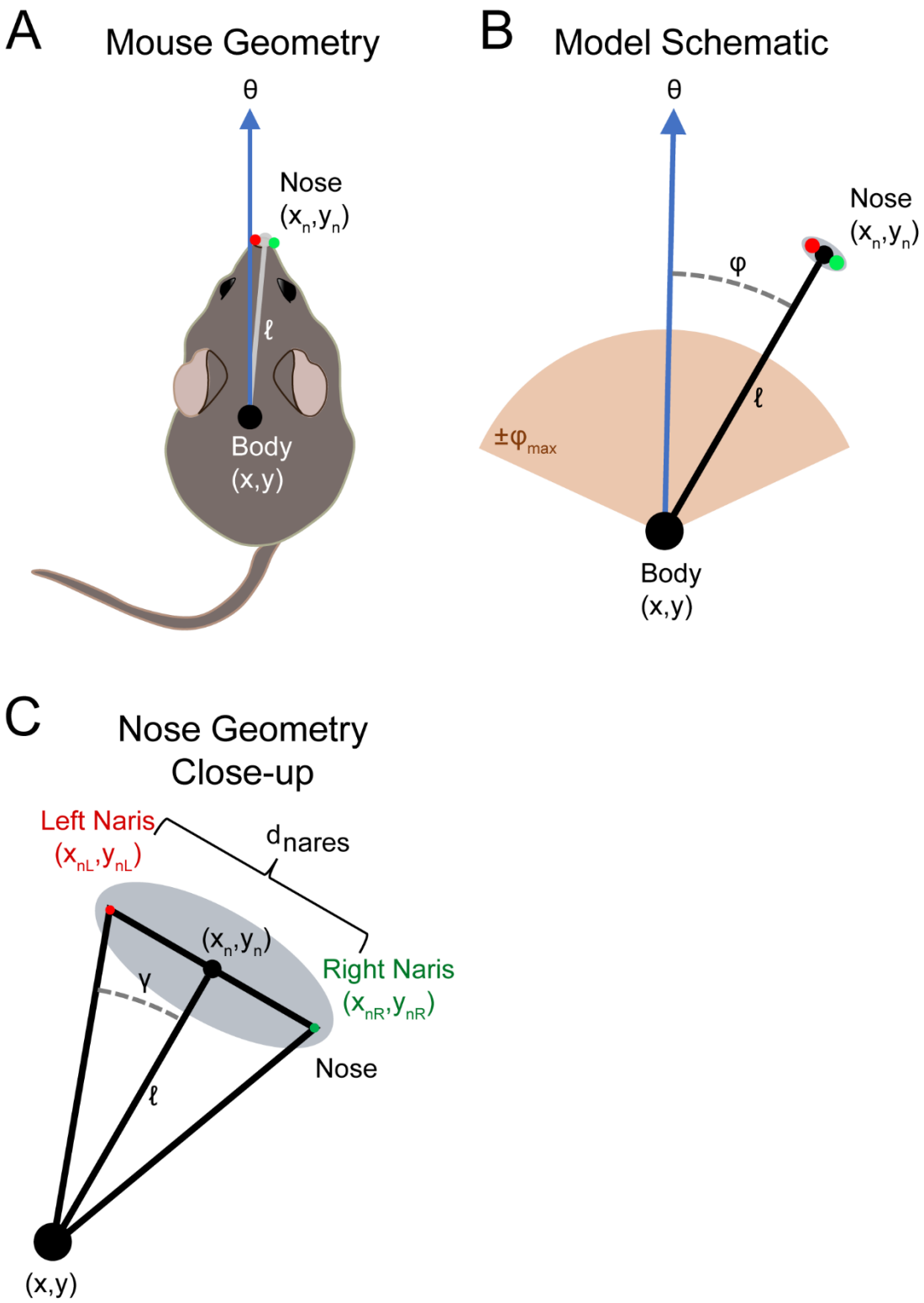

SUPPLEMENTAL TABLE 1

Variable	p value	β value
Experimenter	0.06	-0.63
Baited	**1.95E-14**	**1.81**
Concentration	0.06	0.25
Order of Trial	0.57	0.05
Trial	0.57	0.05
Mouse	**1.41E-3**	**0.22**
Initial Distance	0.11	-7.25E-3
Initial Orientation	0.93	-7.41
Mean Body Velocity	**1.46E-10**	**-0.32**
Mean Nose Velocity	**3.11E-5**	**0.20**
Mean Curvature	**2.13E-5**	**-3.48**
Exploration %	**1.93E-11**	**5.19**
Mean Nose Acceleration	0.03	-0.04

SUPPLEMENTAL TABLE 2

Parameter	p value	β value	Min	Max
ℓ	1.36E-140	0.31	0.01 cm	10
v_{max}	2.93E-19	-0.05	20 cm/s	40
d_{nares}	2.13E-37	1.41	0.01 cm	1
k_{stereo}	1.28E-34	4.44E-3	0.01	300
σ_{max}	7.67E-26	1.59	0.01	1
σ_{min}	1.03E-4	0.66	0.01	1